Struct Chem
DOI 10.1007/s11224-015-0734-1

ORIGINAL RESEARCH

Anion-/cation-directed reaction routes to polymorphic forms of a pyrazole-type ligand and its coordination compounds with zinc. Key structural differences between polymorphs'

Berta Barta Holló[1] · Katalin Mészáros Szécsényi[1] · Mária Deli[2] · Lóránd Kiss[2] · Alfréd Kállay-Menyhárd[3,4] · Vukosava Živković-Radovanović[5] · Zoran D. Tomić[6]

Received: 11 September 2015 / Accepted: 23 December 2015

Abstract Synthetic paths toward the two polymorphs of a monohydrate, one anhydrous polymorph of 1-carboxamidino-5-hydroxy-3-methylpyrazole (*hcmp*) and two polymorphs of zinc complexes containing *hcmp* ligand are presented. By choosing ions which are not part of the final product, it is possible to direct the synthesis toward the particular polymorph. In all three modifications of *hcmp,* the same hydrogen bonding motif appears, leading to formation of similar molecular chains. Differences arise due to different modes of chain aggregation and the presence of solvent water. Analysis of the crystal packing and the energetic features of *hcmp* polymorphs is made using the PIXEL model. The thermal decomposition processes are examined using differential scanning calorimetry and thermogravimetry. Analysis of crystal packing in the two polymorphs of zinc complex suggests the key role of the hydrogen bonding capacity of the aqua ligand for the appearance of the two polymorphic forms. In both polymorphs of zinc complex, stacking interactions have an important role. However, the enhanced hydrogen bonding capacity of the aqua ligand influences the formation of multistacking arrangement.

Keywords Polymorphism · PIXEL calculations · Intermolecular interactions · Pyrazole-based ligand and Zn complex

✉ Zoran D. Tomić
zorant@vin.bg.ac.rs

[1] Faculty of Sciences, University of Novi Sad, Trg Dositeja Obradovica 3, Novi Sad 21000, Serbia

[2] Biological Research Centre HAS, Institute of Biophysics, Szeged, Hungary

[3] Laboratory of Plastics and Rubber Technology, Department of Physical Chemistry and Materials Science, Budapest University of Technology and Economics, Műegyetem rakpart 3. H/1, Budapest 1111, Hungary

[4] Research Center for Natural Sciences, Institute of Materials Science and Environmental Chemistry, Hungarian Academy of Sciences, Magyar tudósok körútja 2, Budapest 1117, Hungary

[5] Faculty of Chemistry, University of Belgrade, P.O. Box 51, Belgrade 11158, Serbia

[6] Laboratory of Theoretical Physics and Condensed Matter Physics, VINČA' Institute of Nuclear Sciences, University of Belgrade, P.O. Box 522, Belgrade 11001, Serbia

Introduction

A large group of pyrazole derivatives and/or their coordination compounds show biological activity [1–4] or anti-inflammatory [5], analgesic [6] or anti-diabetic [7] effect. As the number of pathogens resistant to widely used antibiotics is constantly growing, finding new compounds with a wide spectrum of antimicrobial or antiviral activity but low toxicity toward normal cells is a challenging task. Coordination of biologically active ligands with metal ions often alters the activity that may be enhanced [8, 9] or decreased [10] by complex formation. As our interest in pyrazole-type compounds dates back more than a decade [11–13], the goal of this study was to prepare a potentially bioactive ligand, 1-carboxamidino-5-hydroxy-3-methylpyrazole (*hcmp*), and its complexes in the form of single crystals. The reactions of the ligand were carried out with zinc(II) and magnesium(II) salts in aqueous and ethanolic solutions in order to see how the changes in reaction conditions affect the composition/structure/morphology of the formed compounds. Namely, the bioavailability of the active pharmaceutical ingredients (API) depends not only on its structure, but also on the

Published online: 07 January 2016

physical form. The physical form of API is often determined by the conditions of crystallization, and very often, one compound exists in more than one crystal form [14]. By controlling the nucleation and growth process, nanocrystals with desired composition and morphology may be obtained [15]. Here, depending on the reaction conditions, we obtained two solvatomorphs and the anhydrous form of *hcmp* and two polymorphic complexes of zinc in well-repeatable chemical processes. The crystal structures of the ligand and the zinc complexes were determined. The polymorphism of the ligand in solid state is discussed on the basis of its tautomerism in solution which is supported by spectral data. The desolvation temperatures of the two *hcmp* polymorphs and the thermal decomposition temperatures of the anhydrous forms of *hcmp* have been discussed in view of the energetic analysis of the crystal packing. Analysis of crystal packing in Zn-complex polymorphs has been done with the aim to determine the most significant structural features, which differentiate the two polymorphs. Additionally, the cytotoxicity of the compounds was tested on human intestinal epithelial (Caco-2) cells using viability MTT (with tetrazolium salts) and lactate dehydrogenase (LDH) assays.

Experimental

Materials and measurements

All chemicals were commercial products of analytical reagent grade. The thermogravimetric and differential scanning calorimetric data were recorded on SDT Q600 thermal analyzer, TA Instruments, at a heating rate of 10 °C min^{-1} in nitrogen atmosphere (100 cm^3 min^{-1}) with sample masses of ~3 mg using alumina crucibles. The non-isothermal phase change curves were recorded using a PerkinElmer DSC 7 apparatus. Sample masses were between 3 and 5 mg and measured at 10 °C min^{-1} heating and cooling rates under continuous nitrogen flow (20 cm^3 min^{-1}) in hermetically sealed aluminum pans. The molar conductivity of the freshly prepared DMF solutions of *hcmp* and the complexes was measured on a digital conductivity meter Jenway 4010.

Synthesis of the compounds

1-Carboxamidino-5-hydroxy-3-methylpyrazole (hcmp)

The polymorph *hcmp* (**1**) was obtained by the condensation reaction of aminoguanidine hydrochloride and ethyl acetoacetate in an aqueous solution, in the presence of sodium acetate as described by Erkin and Krutikov [16], and crystallized in the form of monohydrate. As one of our aims was to prepare a complex of *hcmp* with Mg^{II}, the complex formation reaction was carried out using $MgCO_3$. However, instead of the corresponding complex, *hcmp* crystallized in the form of polymorph **2** that was prepared by the following procedure. 1 mmol (0.16 g) *hcmp* was dissolved in water at 90 °C. To the warm solution of *hcmp* (1 mmol), solid $MgCO_3$ (1 mmol) was added. The mixture was refluxed for 10 min at 90 °C, and then glacial acetic acid was added dropwise until the dissolution of $MgCO_3$. The pH of the reaction mixture was set to 10 by ammonia solution drops and left at room temperature. After 2–3 days, yellowish single crystals were obtained and filtered off. In this way, *hcmp* crystallizes with one water molecule. Solvent change from water to ethanol in the same synthetic procedure resulted in formation of anhydrous *hcmp* (**3**). The crystallization at room temperature takes about 3 weeks. Yields: 84 % (**1**), 32 % (**2**) and 10 % (**3**). M_r ($C_5H_{10}N_4O_2$) = 158.16 g mol^{-1}. All crystalline ligand types are well soluble in DMF and DMSO at room temperature and partly soluble by heating in EtOH and water. Λ_M(DMF) = 1.0 S cm^2 mol^{-1}.

[Zn(hcmp–H)$_2$H$_2$O]

To prepare complex of Zn^{II} with *hcmp*, the ligand-to-metal molar ratio was varied in 3:2, 2:1 and 1:1 proportions. The optimal ligand-to-metal molar ratio for the complexation with Zn^{II} was 2:1 in an ethanolic solution. The reaction was carried out by the mixing of zinc(II) salt (0.5 mmol) dissolved in 5 cm^3 EtOH with a solution of *hcmp* (1 mmol) in 15 cm^3 EtOH by heating and intensive stirring. After standing for 24 h at room temperature, to the reaction mixture 3 cm^3 of ammonia solution was added. The addition of ammonia solution promoted the deprotonation of the ligand, namely the precipitation of the neutral complex. At the same time, as a result of zinc ammine formation, the concentration of Zn^{II} is lowered, assisting thus the single-crystal formation. In 2–3 days, single crystals were formed from the solution containing $ZnCl_2$ (uncolored), $ZnBr_2$(light orange) and $Zn(NO_3)_2$ (light yellow). With $ZnBr_2$ and $ZnCl_2$, the ligand coordinates to form polymorph **I**. Differently, with $Zn(NO_3)_2 \cdot 6H_2O$ the polymorph **II** was obtained. The precipitates were filtered off and washed with EtOH. Yields: >85 % for **I** and >81 % for **II**. Both polymorphs, $M_r(ZnC_{10}H_{16}N_8O_3)$ = 361.68 g mol^{-1}, are well soluble in DMSO and DMF at mild heating, but in common solvents as EtOH, MeOH, water or acetone, the complexes are hardly soluble. Λ_M(DMF) = 1.9 S cm^2/mol.

Crystal structure determination and refinement

Single-crystal X-ray diffraction data of compounds **1–3** and **I–II** were collected on an Oxford Diffraction Gemini S

four-circle diffractometer equipped with a Sapphire CCD detector, using CuKα radiation (λ = 1.54184 Å) at room temperature. The data reduction was done using the Oxford Diffraction program CrysAlisPro [17]. Empirical absorption correction using spherical harmonics implemented in the SCALE3 ABSPACK [18] scaling algorithm were applied for compounds **1**, **3**, **I** and **II**. Numerical absorption correction using a multifaceted crystal model, as implemented in CrysAlisPro [17] program system, was applied for compound **2**. The structures were solved by direct methods using SIR92 program [19] as implemented in WinGX program system [20]. Compound **3** crystallizes in space group $P2_12_12_1$, but it is a weak anomalous scatterer, and the absolute structure cannot be determined reliably from the Flack parameter. All non-hydrogen atoms were refined anisotropically using SHELXL-97 [21] by applying a full-matrix least-squares method based on F^2, including all reflections. The hydrogen atoms belonging to the methyl group in **1** were located from difference electron-density map, for **2**–**3** and **I**–**II** methyl hydrogens are generated at ideal positions. The hydrogen atoms belonging to the nitrogen atoms, and pyrazole ring carbon atom, were found in the difference electron-density maps. All hydrogen atoms were refined using riding model. The molecular diagrams were generated using ORTEP-3 for Windows [22]. For packing diagrams, the programs CAMERON [23] and Mercury [24] were employed. Geometrical calculations were carried out using the program PLATON [25]. The crystal data and refinement parameters are summarized in Table 1. In the amidine fragment, C1–N1/C1–N2 bond lengths are 1.310(2)/1.313(2), 1.312(2)/1.309(2) and 1.318(5)/1.301(5) Å in molecules of **1**, **2** and **3**, respectively. Close similarity of two C–N distances indicates that amidine fragment is protonated and exists in two resonant forms (Scheme 1). Consequently, *hcmp* in all three modifications exists in the form of zwitterion with negative charge located on the pyrazolone-O and positive charge located at the protonated amidine fragment.

Calculation of intermolecular energies

Molecule–molecule pairwise energies in **1**–**3** were calculated by the CLP program package [26] (version 12.5.2014). Crystal coordinates were used for non-hydrogen atoms, while the H atoms were normalized using the RETCIF module of the CLP software [26]. Molecular electron-density calculations of **1**–**3** were performed in Gaussian 09 [27] at the MP2/6-31G (d,p) level. These electron densities were used to calculate intermolecular interaction energies in **1**–**3** by the PIXEL [28] method using a distance cutoff from the central molecule of 30 Å. The positions of atoms for the purpose of this calculation were obtained using RETCIF and RETCOR modules of the CLP software.

Materials and methods for biological activity studies

All reagents were purchased from Sigma-Aldrich Kft., Hungary, unless otherwise indicated. Phosphate buffer solution (PBS, pH 7.4) and Dulbecco's modified Eagle's medium (DMEM) were purchased from Gibco, Invitrogen. Fetal bovine serum from Lonza, Switzerland. Cytotoxicity detection kit measuring lactate dehydrogenase (LDH) release from Roche, Switzerland. Ninety-six-well cell culture plates form Orange, UK. Solubility measurements, cell culture and the viability assays are described in detail in the Supporting Material.

Discussion

The synthesis and the structure, determined by spectroscopic methods, of *hcmp* are published earlier [16]. The crystal structures of the two polymorphs of a monohydrate and the solvent-free form obtained by different, well-repeatable synthetic procedures are described for the first time here. It is known that in ionic salts, anion participates in molecular self-assembly in coordination compounds [29]. Our results refer to the significant role of the anion in the crystallization process affecting the symmetry of the crystal even when it is not a part of the molecule. The molar conductivity values in DMF solution of the ligands **1**–**3** (1.0 S cm^2 mol^{-1}) and the complexes **I** and **II** (1.9 S cm^2 mol^{-1}), in accordance with the structure, refer to their non-electrolytic character [30].

Crystal and molecular structures of the ligand

A perspective view and atom numbering scheme of **1** is shown in Fig. 1. The same labeling scheme is applied for the polymorph **2** and the solvent-free form **3**.

Geometry of the selected nonbonding contacts is given in Table 2.

According to its ^{1}H NMR and IR spectrum [16], 5-hydroxy-1-carboxamidino-3-methylpyrazole (*hcmp*) in solution exists predominantly in the lactim form (Scheme 1a) with strong interaction between hydroxyl and imino groups. However, in the crystal structure of all three polymorphic modifications, the amidine moiety is protonated and *hcmp* exists as zwitterion with two resonance forms (Scheme 1b, c).

Bond lengths of *hcmp* in all three polymorphic modifications are similar. All interatomic distances can be considered normal, and the pyrazole rings are planar within experimental error. The only significant variation in the molecular geometry is the rotation of the carboxamidine group relative to pyrazole ring. Dihedral angle between the mean planes of the pyrazole ring and carboxamidine group

Table 1 Crystal data and structure refinement for compounds **1–3**, **I** and **II**

	1	**2**	**3**	**I**	**II**
Empirical formula	$C_5H_8N_4O{\cdot}H_2O$	$C_5H_8N_4O{\cdot}H_2O$	$C_5H_8N_4O$	$C_{10}H_{16}N_8O_3Zn$	$C_{10}H_{16}N_8O_3Zn$
Formula weight	158.17	158.17	140.15	361.70	361.70
Wavelength (Å)	1.54184	1.54184	1.54184	1.54184	1.54184
Crystal system	Monoclinic	Orthorhombic	Orthorhombic	Monoclinic	Monoclinic
Space group	P21/*n*	Pbca	$P2_12_12_1$	$P2_1/c$	$P2_1/n$
a (Å)	7.8258(3)	12.4996(4)	7.767(5)	10.5350(2)	8.8637(3)
b (Å)	11.5640(5)	9.8078(4)	8.102(5)	13.0020(4)	7.3260(2)
c (Å)	8.7744(3)	12.8102(5)	10.966(5)	11.0961(2)	23.3707(7)
α (°)	90	90	90	90	90
β (°)	102.929(4)	90	90	96.168(2)	98.550(3)
γ (°)	90	90	90	90	90
V (Å^3)	773.93(5)	1570.5(1)	690.1(7)	1511.10(6)	1500.72(8)
Z	4	8	4	4	4
D_{calc} (g/cm^3)	1.357	1.338	1.349	1.590	1.601
μ (CuKα) (mm^{-1})	0.908	0.895	0.841	2.514	2.531
F(000)	336	672	296	744	744
θ range (°)	6.4–72.3	6.7–72.4	6.8–72.1	4.2–72.5	3.8–72.5
Ref. collected	2602	3774	1477	5525	5287
Unique ref. (R_{int})	1485 (0.023)	1528 (0.023)	1134(0.013)	2920(0.020)	2891(0.028)
Data/parameters	1485/101	1528/102	1134/92	2920/201	2891/201
GOF on F^2	1.07	1.05	1.08	1.05	1.04
wR (all data)	0.1182	0.1212	0.1246	0.0933	0.1142
R (all data)	0.0393	0.0486	0.0536	0.0399	0.0507
Residual density (e/Å^3)	−0.17/0.20	−0.22/0.24	−0.15/0.13	−0.25/0.26	−0.36/0.41
CCDC No.	1002039	1002040	1002192	1002041	1002042
Pack. coefficient	67.3	66.2	66.0	68.2	68.7

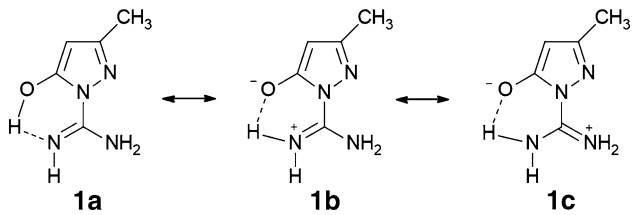

Scheme 1 Tautomeric and resonant forms of *hcmp*

is 0.53°, 5.76° and 12.31° in **1**, **2** and **3**, respectively. Intramolecular energies, as calculated in Gaussian 09 [27] at the MP2/6-31G(d,p) level, indicate that intramolecular energy of **1** is higher for 4.63 and 15.18 kJ/mol relative to **2** and **3**, respectively. Inspection of nonbonding interactions involving the carboxamidine group in **1–3** indicates that this difference is associated with different environment of carboxamidine group (Table 2). In the solvatomorphic forms **1** and **2**, the protonated carboxamidine group is hydrogen-bonded to the two molecules of water and one *hcmp* molecule. In anhydrous form **3**, the carboxamidine group interacts with two molecules of *hcmp*. It can be

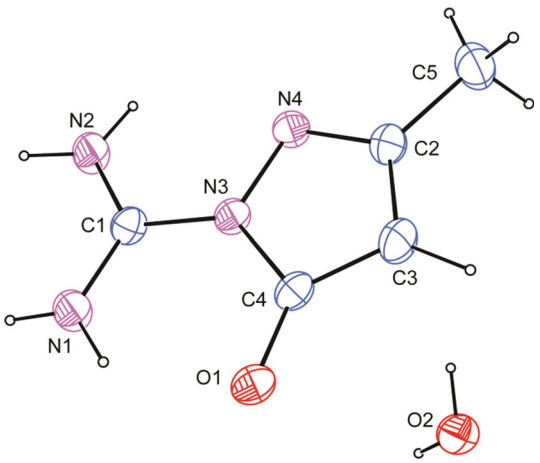

Fig. 1 View of asymmetric unit of **1**. Same labeling scheme is applied for the polymorph **2** and the solvent-free form **3**

therefore assumed that the steric effects, dependent on the type of surrounding molecules (water or *hcmp*), influence the orientation of the carboxamidine group. It should be

Table 2 Geometry of the selected nonbonding contacts in **1–3**

D–H···A	H···A(Å)	D–H···A(°)	D···A(Å)	Symmetry code
1				
N2–H4···O1	1.92	172	2.814(2)	$-1/2+x$, $1/2-y$, $1/2+z$
O2–H10···N4	2.09	159	2.893(2)	$3/2-x$, $1/2+y$, $1/2-z$
O2–H9···O1	1.89	165	2.759(2)	$1/2+x$, $1/2-y$, $1/2+z$
N2–H3···O2	2.11	151	2.917(2)	$-1/2+x$, $1/2-y$, $1/2+z$
N1–H2···O2	1.99	173	2.880(2)	$-1+x$, y, z
N1–H1···O1	1.97	131	2.673(2)	
Stacking interactions				
*Cg*1···*Cg*1(Å)	3.6922(9)			$1-x$, $-y$, $-z$
2				
N2–H4···O1	1.96	165	2.835(2)	x, $1/2-y$, $1/2+z$
O2–H10···N4	2.04	164	2.897(2)	
N1–H2···O2	2.00	171	2.880(2)	$-1/2+x$, $1/2-y$, $1-z$
N2–H3···O2	2.04	157	2.930(2)	$1-x$, $-y$, $1-z$
O2–H9···O1	1.87	162	2.717(2)	$1/2+x$, y, $1/2-z$
N1–H1···O1	1.97	135	2.678(2)	
3				
N1–H2···O1	1.88	173	2.766(4)	$1-x$, $-1/2+y$, $1/2-z$
N2–H3···O1	1.92	155	2.798(4)	$1/2-x$, $-y$, $-1/2+z$
N2–H4···N4	2.32	151	3.064(5)	$1/2+x$, $-1/2-y$, $-z$
N1–H1···O1	1.98	133	2.684(4)	

*Cg*1 refer to the centroid of the ring formed by C2–C3–C4–N3–N4

noted that conformational flexibility of the $-C(NH_2)_2$ group is partly reduced by the intramolecular hydrogen bond N1–H1…O1 (Table 2) which is present in all three forms of *hcmp*. Aggregation of molecules in polymorphs **1** and **2** is achieved through the same hydrogen bonding motifs (Table 2), and the same 1D supramolecular motif, molecular chain, is formed (Fig. 2a). The molecules of *hcmp* are directly connected through the N2–H4···O1 H-bonds and also via the hydrogen bonds involving solvent water molecule (N1–H2•••O2 and O2–H9•••O1) forming chains of molecules related by a glide plane. The similarity of the molecular chains formed in **1** and **2** is reflected in the mutual orientation of the consecutive pyrazole moieties. Thus, dihedral angle between the mean planes of the neighboring pyrazole rings within the same chain is 75.1° and 75.8° in compounds **1** and **2**, respectively. This similarity is illustrated in Fig. 2, where the parts of the crystal structures of **1** (black) and **2** (gray) are overlaid. Connection between the neighboring chains in both **1** and **2** is achieved through the interactions of *hcmp* with water (Table 2; Fig. 2b, c). While the intrachain geometry and associated intermolecular contacts show close similarity in polymorphs **1** and **2**, aggregation of these chains into the crystal lattice differentiate the two structures. In **1** (Fig. 2b), *hcmp* molecules from the neighboring chains are oriented in an antiparallel fashion, giving rise to stacking interaction with a centroid-to-centroid separation of 3.69 Å. Dissimilar to **1**, the *hcmp* molecules from the neighboring chains in **2** (Fig. 2c) are mutually rotated forming the torsion angle O1–Cg–Cg*i*–O1^i of 131.73°, while the closest centroid-to-centroid separation increases to 6.27 Å (Fig. 2c; $i = 1/2 + x$, y, $1/2–z$; *Cg*1 designate centroid of the ring C2–C3–C4–N3–N4). The closer approach of the *hcmp* rings in the structure **1** is probably facilitated by the hydrogen bonding involving two water molecules (Fig. 2b) and O1 and N4 acceptors of stacked rings. This is not the case with **2** where only one water molecule is situated between the rings.

In polymorph **3**, basic supramolecular motif could be also described as molecular chain, formed by the propagation of the same type of hydrogen bonds as in **1** and **2**, the N2–H3···O1 (Fig. 3b). Molecules in the chain are related by a screw axis and arranged in the crystallographic *c* direction. Dihedral angle between the mean planes of the neighboring pyrazole rings within the same chain is 73.59°, not significantly different from **1** and **2**. Neighboring chains are linked through the N–H···O and N–H···N H–bonds (Fig. 3a; Table 2).

In summary, it can be said that in polymorphs **1**, **2** and **3**, the basic supramolecular motif, common to all three structures, is a molecular chain formed by the N–H···O hydrogen bonds. What makes the difference between the

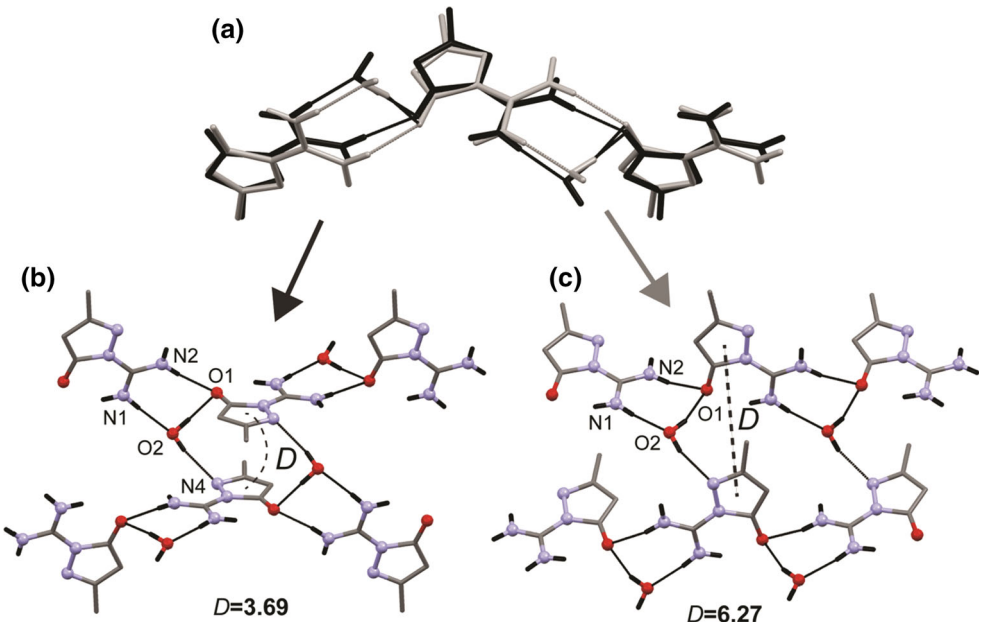

Fig. 2 Overlay diagram of molecular chains (**a**) in **1** (*black*) and **2** (*gray*) depicting the similarity of the intrachain geometry. Part of the crystal structure illustrating different orientation of neighboring chains in **1** (**b**) and **2** (**c**). *Dashed line* indicates closest ring–ring separation (**d**) between the neighboring chains

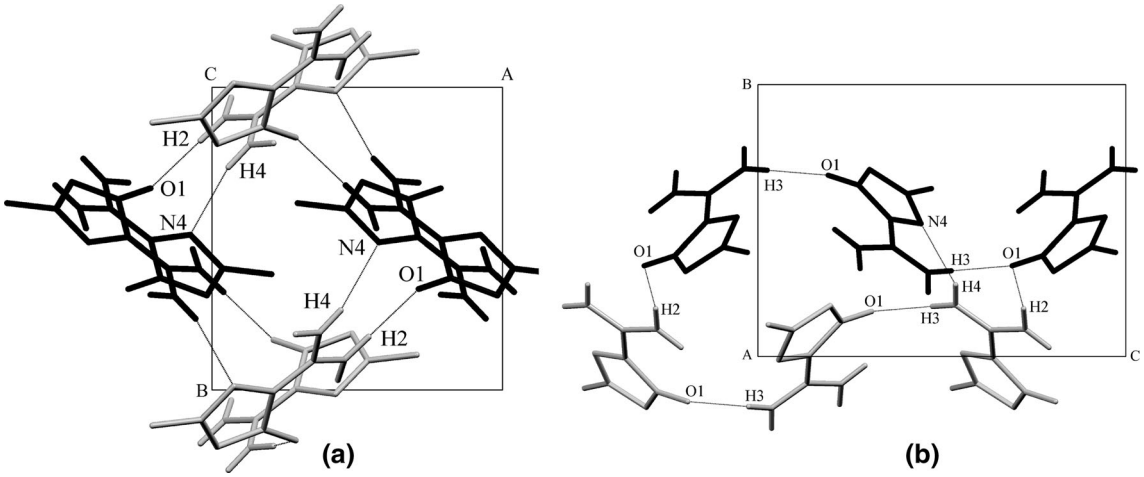

Fig. 3 Crystal packing of 3. View down the c axis (**a**) shows arrangement of molecules into chains and interchain links. View down the a axis (**b**) depicts details of intrachain and interchain connections

three modifications is the way these chains connect into crystal structure. The above observations pose two questions: Does these structural differences in the aggregation of molecular chains lead to significant difference in the stability of the crystal, and what is the relative importance of various nonbonding contacts for the formation of particular molecular arrangement in the crystal? In order to investigate the significance of nonbonding contacts for the aggregation of molecules, common approach is to compare observed geometrical properties with a vast quantity of empirical data related to the geometry of intermolecular contacts [31]. However, ranking the contacts observed in a particular structure in terms of their importance while relaying only on geometrical criteria is complicated by the presence of a number of close nonbonding atom–atom contacts. These contacts often have similar geometrical features, and there are no clear criteria for connecting the particular structural features with its significance in the process of molecular aggregation. One of the methods to overcome this problem is quantitative evaluation of crystal lattice energy and partition of energy into pairwise molecule–molecule contributions [32]. To gain more insight into the relative importance of various nonbonding contacts, pairwise molecule–molecule energies of **1**–**3** were calculated using PIXEL method implemented in CLP program [26, 34]. To identify the most significant intermolecular contacts, we looked at the molecule–molecule energies. Interaction energies of the selected molecular

pairs, partitioned into electrostatic (Coulombic, E_C), polarization (E_P), dispersion (E_d) and repulsive (E_r) contributions, together with associated intermolecular contacts, are given in Table 3. In polymorphs **1**–**3**, the largest interaction energy corresponds to the hydrogen bond formed between the pyrazolone oxygen and amino hydrogen. In **1** and **2**, the molecular chains are formed through the *hcmp*···*hcmp* and *hcmp*···H_2O interactions. Connection between the molecular chains is achieved through the interaction of *hcmp* with water. In **3**, *hcmp* molecules are linked directly and pack in a herringbone fashion. The packing coefficients [33] are not significantly different in **1**, **2** and **3** (Table 1). Due to the zwitterionic nature of the molecule (Scheme 1), dominant contribution to the strongest intermolecular interaction comes from the coulombic term (Table 3). Partition of the total energy of pairwise interactions indicates that electrostatic forces are dominant in other intermolecular contacts, too. The only exception to this is stacking interaction of *hcmp* molecules in **1** (Tables 2, 3). In this case, dominant contribution to the intermolecular energy comes from dispersion forces, while the coulombic energy has a positive sign and destabilizes the stacking arrangement. The largest energy of intermolecular interaction in **3** is somewhat lower than the largest energy observed in **1** and **2**. However, the second largest energy of interaction in **3** is larger than the second largest energy found in **1** and **2**.

It should be noted that the presence of stacking interactions supported by two pairs of hydrogen bonds involving water did not lead to larger temperature of dehydration in **1**, in comparison to **2** where the stacking interactions are absent.

Crystal and molecular structures of the complexes I and II

Coordination of *hcmp* to Zn in the presence of chloride or bromide ions leads to the formation of [Zn(*hcmp*–H)$_2$H$_2$O] in the polymorphic form **I**. If nitrate ion is used instead, the polymorph **II** is formed. In complexes **I** and **II**, the Zn atom is five-coordinated with two *hcmp* ligands bonded through the N4 atom of pyrazole ring and amidinium nitrogen N2. The fifth position is occupied by a water molecule (Fig. 4a).

The Addison distortion index τ [35] ($\tau = 0$ for a square pyramid and $\tau = 1$ for a trigonal bipyramid) is 0.84 and 0.72 for complex molecules **I** and **II**, respectively. Hence, for both **I** and **II**, the coordination geometry is best described as distorted trigonal bipyramid. Similarity of the molecular geometries in polymorphs **I** and **II** is evident from the comparison of relevant bonds and angles. Overlay of the molecules (Fig. 4b) of **I** (red) and **II** (green) illustrate the similarity of the molecular shape. Hence, both complexes have similar capacity for the formation of

Table 3 PIXEL [32] interaction energies (kJ/mol) in the crystals **1**–**3**, between molecular pairs related by a symmetry code, and the associated intermolecular contacts

Molecular pair	E_{coul}	E_{pol}	E_{disp}	E_{rep}	E_{tot}	Associated intermolecular contacts*	Symmetry code
1							
hcmp···*hcmp*	−73.2	−23.3	−15.6	47.9	−64.2	N2–H4···O1	−1/2+*x*, 1/2−*y*, 1/2+*z*
hcmp···H_2O	−51.5	−23.4	−17.9	58.3	−34.4	O2–H10···N4	3/2−*x*, 1/2+*y*, 1/2−*z*
hcmp···H_2O	−50.0	−20.3	−10.3	54.9	−25.7	O2–H9···O1	1/2+*x*, 1/2−*y*, 1/2+*z*
hcmp···H_2O	−23.9	−9.3	−7.8	19.0	−22.0	N2–H3···O2	−1/2+*x*, 1/2−*y*,1/2+*z*
hcmp···H_2O	−30.3	−16.1	−10.9	35.6	−21.7	N1–H2···O2	−1+*x*, *y*, *z*
hcmp···*hcmp*	4.2	−5.6	−26.6	10.3	−17.7	Cg1···.Cg1	1−*x*, −*y*, −*z*
2							
hcmp···*hcmp*	−72.6	−22.3	−15.1	42.8	−67.2	N2–H4···O1	*x*, 1/2−*y*,1/2+*z*
hcmp···H_2O	−48.7	−22.4	−16.0	53.7	−33.4	O2–H10···N4	
hcmp···H_2O	−34.3	−15.9	−10.2	34.0	−26.3	N1–H2···O2	−1/2+*x*, 1/2−*y*, 1−*z*
hcmp···H_2O	−25.5	−12.0	−9.0	23.4	−23.2	N2–H3···O2	1−*x*, −*y*, 1−*z*
hcmp···H_2O	−47.4	−23.0	−11.0	62.2	−19.2	O2–H9···O1	1/2+*x*, *y*, 1/2−*z*
3							
hcmp···*hcmp*	−74.2	−28.5	−17.0	58.1	−61.6	N1–H2···O1	1−*x*, −1/2+*y*, 1/2−*z*
hcmp···*hcmp*	−57.9	−23.1	−20.8	43.7	−58.1	N2–H3···O1	1/2−*x*, −*y*, −1/2+*z*
hcmp···*hcmp*	−26.4	−15.7	−17.4	24.5	−35.0	N2–H4···N4	1/2+*x*, −1/2−*y*, −*z*

Cg1 refers to the centroid of the ring formed by C2–C3–C4–N3–N4

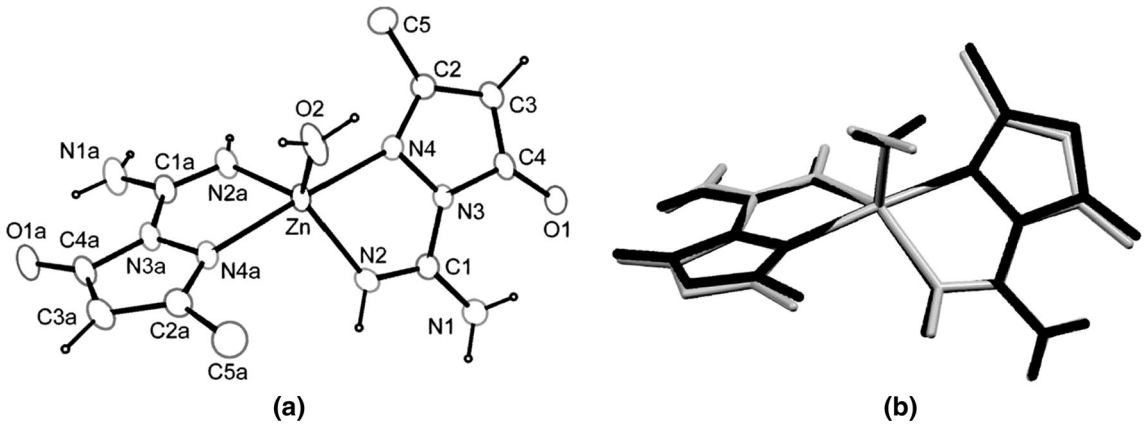

Fig. 4 **a** ORTEP view of **I**. The atom labeling schemes in **I** and **II** are identical. Methyl hydrogens have been removed for clarity. **b** Overlay of molecular structures in **I** (*black*) and **II** (*gray*)

intermolecular interactions. The most notable difference in the molecular geometry of **I** and **II** is the orientation of the coordinated water molecule relative to the Zn–O2 bond (Fig. 5). In complex **I**, the water molecule is oriented so that angle between the mean plane of the water atoms and Zn–O2 bond is 0.4(2)°. In **II**, water molecule is tilted relative to Zn–O2 bond and the associated angle is 40.4(2)°. This difference influences the capacity of coordinated water for intermolecular bonding since, due to the steric factors, oxygen is more easily accessible for neighboring molecules in **II** than in **I**. This is reflected in the type and geometry of intermolecular contacts. Geometry of the selected nonbonding contacts in **I** and **II** is given in Tables 4 and 5. In **I**, water is hydrogen-bonded to two neighboring molecules through the O2–H2···O1 and O2–H2a···O1a H-bonds. In **II**, water is involved in same hydrogen bonding motif with two neighboring molecules, but additionally accepts hydrogen bond from the third molecule N1–H2…O2. Difference in the position of coordinated water and the associated hydrogen bonds are depicted in Fig. 5.

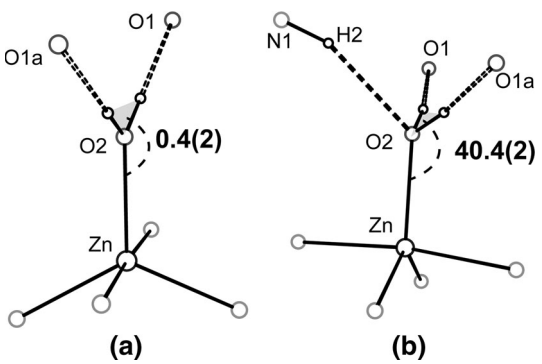

Fig. 5 Details of crystal structures of I (**a**) and II (**b**) showing different orientation of the coordinated water relative to Zn–O bond. Relevant hydrogen bonding is depicted as *dashed lines*

In **I**, water is hydrogen-bonded to pyrazolone oxygen of the two neighboring molecules. Both pyrazole rings of a complex molecule are involved in stacking interactions with ring–ring distances of 3.478(1) and 3.464(2) Å (Fig. 6). Propagation of this interaction leads to the aggregation of molecules into chains running along the crystallographic a direction. Neighboring molecular chains are connected through the N–H···O H-bonds (Tab 5, Fig. 7).

In polymorph **II**, coordinated water serves as a donor of hydrogen bonds toward the two neighboring molecules as in polymorph **I**. But dissimilar to **I**, it also serves as an acceptor of hydrogen bond from the third molecule (N1–H…O2) (Fig. 8, colored in black). In the resulting arrangement, only one of the pyrazole rings forms stacking contact similar to **I** (Fig. 8, $\pi 2$), while hydrogen-donating molecule (Fig. 8, colored in black) is involved in the additional stacking arrangement (Fig. 8, $\pi 1$). These stacking interactions ($\pi 1$, $\pi 2$, Fig. 8) propagate in the crystallographic b direction (Fig. 9). Hence, interplay of N2–H3•••O1a, O2–H8•••O1a and stacking interactions lead to formation of multistacked chain of molecules. Neighboring chains are connected through the N1–H2•••O2, N1a–H2a•••O1 and O2–H9•••O1 H-bonds (Fig. 9).

Thermal data of the compounds

The bioavailability of pharmaceuticals strongly depends on its solubility that, in turn, depends on the corresponding crystalline form. DSC studies of polymorphs are especially useful to detect and quantify polymorphism [36] or to determine the transitions between the different polymorphic forms [37]. Even the solubility of a solid may be measured as a function of temperature by differential

Table 4 Geometry of selected intermolecular contacts in **I**

D–H···A	H···A(Å)	D–H···A(°)	D···A(Å)	Symmetry code
N1–H2···O1^{i}	2.26	159	3.124(3)	i = x, 1/2−y, −1/2+z
N1a–H2a···O1a^{i}	2.19	164	3.109(3)	i = x, 1/2−y, −1/2+z
O2–H8···O1a^{ii}	1.89	176	2.699(3)	ii = 1−x, −y, −z
O2–H9···O1^{iii}	1.81	177	2.670(3)	iii = 2−x, −y, 1−z
Stacking interactions				
π1 [Cg1···Cg1^{iv} = 3.478(1) Å]				iv = 2−x, −y, 1−z
π2 [Cg2···Cg2^{v} = 3.464(2) Å]				v = 1−x, −y, −z

Cg1 and Cg2 are the centroids of pyrazole rings N3–C4 and N3a–C4a, respectively

Table 5 Geometry of selected intermolecular contacts in **II**

D–H···A	H···A(Å)	D–H···A(°)	D···A(Å)	Symmetry code
N1–H2···O2^{i}	2.19	158	3.058(3)	i = x, −1+y,z
N1a–H2A···O1^{ii}	2.08	162	2.950(3)	ii = −1/2−x, 1/2+y, 1/2−z
N2–H3···O1a^{iii}	2.19	165	3.108(3)	iii = −x, −y, 1−z
N2A–H3a···O1^{ii}	2.49	145	3.318(3)	ii = −1/2−x, 1/2+y, 1/2−z
O2–H8···O1a^{iv}	1.80	164	2.619(3)	iv = −x, 1−y, 1−z
O2–H9···O1^{v}	1.82	169	2.668(3)	v = 1/2−x, 1/2+y, 1/2−z
Stacking interactions				
π2 [Cg3···Cg3^{vi} = 3.620(2)]				vi = −x, −y, 1−z
π2 [Cg3···Cg3^{vii} = 3.742(2)]				vii = −x, 1−y, 1−z

Cg3 is the centroid of pyrazole ring N3a–C4a

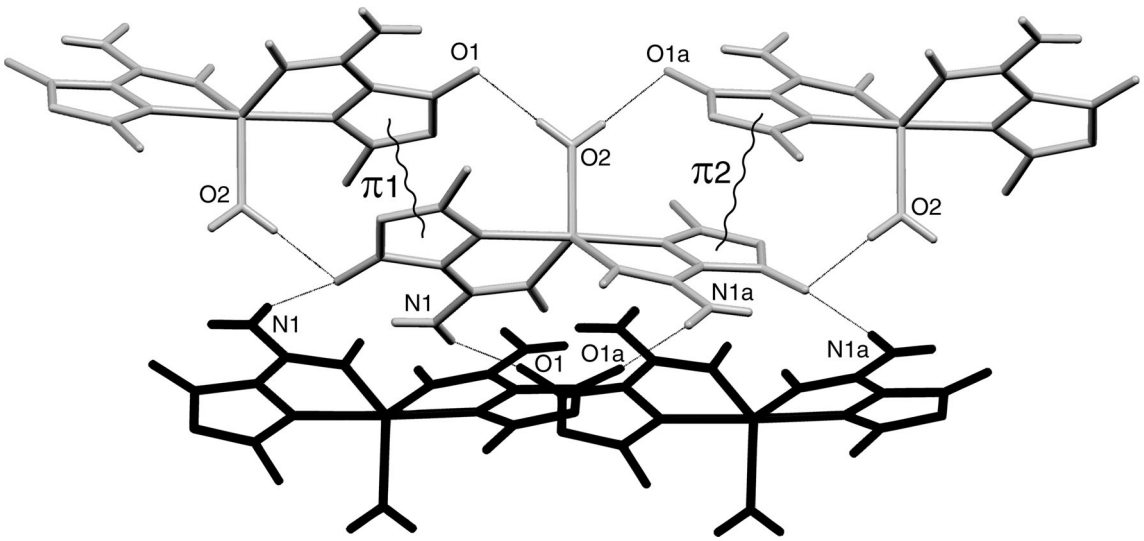

Fig. 6 View of the crystal packing of I showing the formation of two molecular chains (colored in *black* and *gray*). Hydrogen bonds and stacking interactions (π1, π2) are depicted in *dotted* and *waved lines*, respectively

scanning calorimetry of the saturated solution. Here, we used simultaneous thermogravimetric/differential scanning calorimetric (TG/DSC) measurements to compare the thermal decomposition temperatures and the possible phase transitions between polymorphic forms of compounds **1**–**3** and **I**–**II**. For the sake of comparison, DTG/DSC curves were used for the corresponding compounds. In Fig. 10, the thermal decomposition of different forms of the ligand is depicted, while Fig. 11 shows the comparison of the thermal behavior of the complexes.

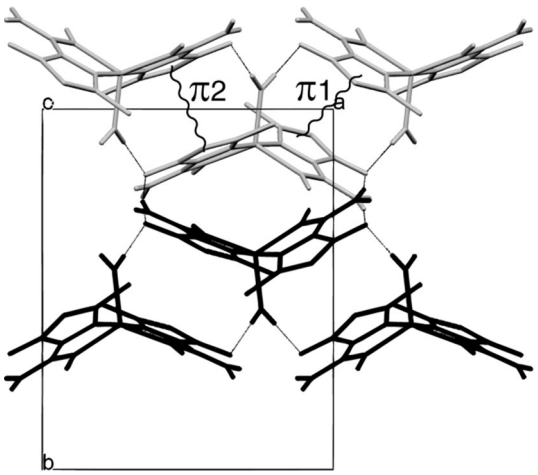

Fig. 7 View of crystal packing in **I** down axis c showing the arrangement of molecular chains

Monohydrates **1** and **2** loose the crystal water below 100 °C. The amount of water corresponds to the stoichiometric quantity (calcd: 11.39 %): 10.5 and 11.1 % in **1** and **2**, respectively. The DTG and DSC maximum for dehydration in compound **2** appear at a little higher temperature (ca. 5 °C, see Fig. 10). After water evaporation, the dehydrated ligands are stable and decompose at DTG onset temperatures of 249 and 243 °C in **1** and **2**, respectively. The anhydrous ligand **3** is stable to 226 °C. Above 350 °C, the decomposition of **1**–**3** in nitrogen is practically finished with about 25 % tar residue.

In principle, some of the polymorphic transitions may be reversible. However, such transition between **1** and **2** in the measured temperature range is not detected. Neither is visible the melting of the compounds. The steep start in DSC curve above 200 °C may refer to melting, but

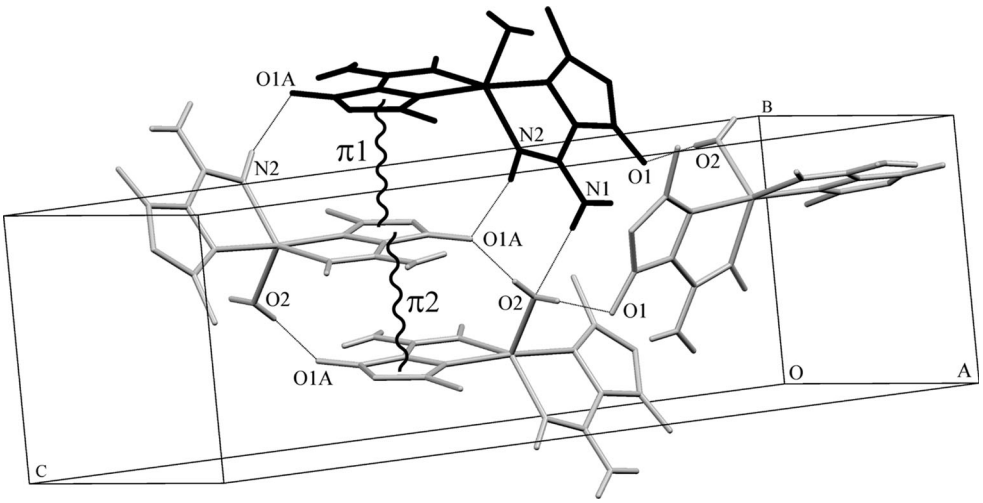

Fig. 8 View of the crystal structure of **II**, showing the significant hydrogen bonds and formation of multistacked chain

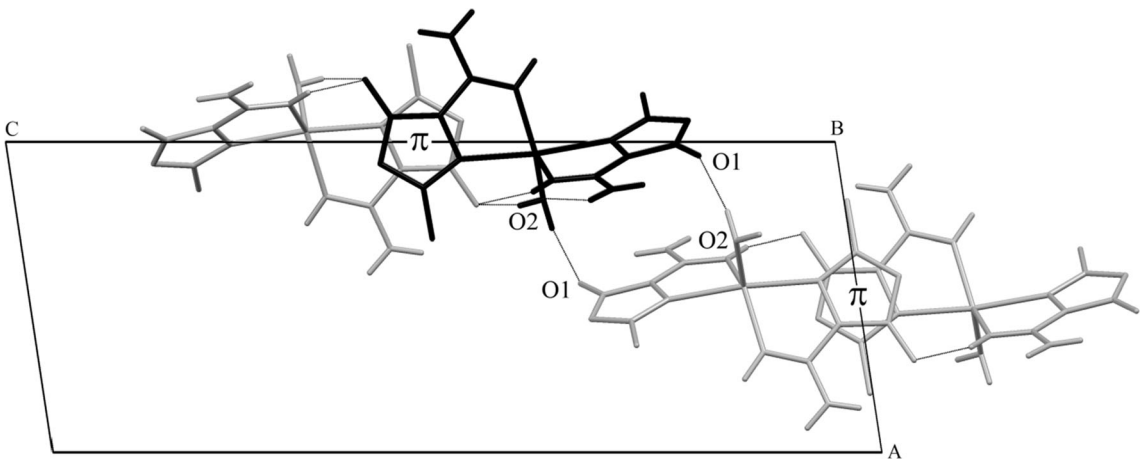

Fig. 9 Formation of molecular chains in **II** and connections between them. Regions involved in multistacked interactions are labeled with π

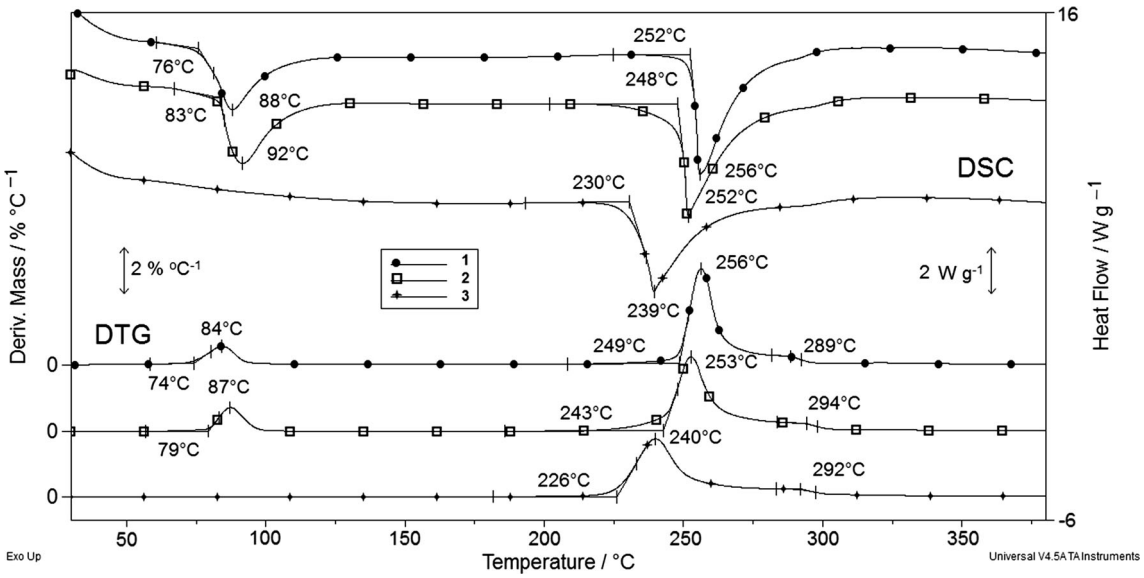

Fig. 10 DTG and DSC curves for the ligand forms **1**–**3**

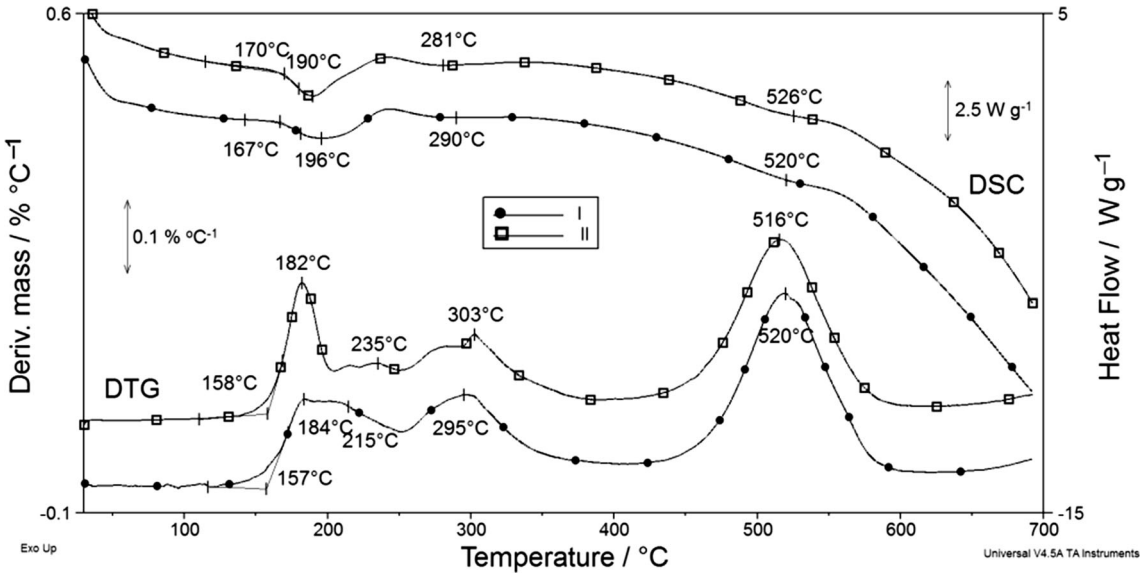

Fig. 11 DTG and DSC curves for complexes **I** and **II**

according to the corresponding DTG curves it is accompanied by decomposition.

In complexes **I** and **II**, the trigonal bipyramidal environment around zinc is established by NN-coordination of two mono-deprotonated *hcmp* ligand molecules and an aqua ligand. However, the high decomposition temperature (Fig. 11) suggests that water molecules are not present. TG/MS measurements (see ESI) support this observation. Namely, despite the coordination of H_2O, it evaporates at room temperature during the storage. Water can be detected in the freshly prepared compound only. The anhydrous complexes have practically the same decomposition temperature (DTG onset 157–158 °C). The only significant difference in decomposition scheme is in the rate of the first decomposition step that is somewhat higher in **II**. The decomposition is not completed up to 700 °C. There is no sign of phase transition between the polymorphs. The comparison of the decomposition mechanism of the ligands and the complexes can be found in ESI.

In order to trace the phase transitions in solvatomorphs, DSC measurements were taken in the temperature range from 50 to −50 °C for all the forms of the ligand as well as for the complexes. On heating, **2** shows an endothermic solid–solid phase transition at −1.6 °C peak temperature (see Fig. 12). On cooling **2** far below the equilibrium temperature (temperature range −25 and −45 °C), several

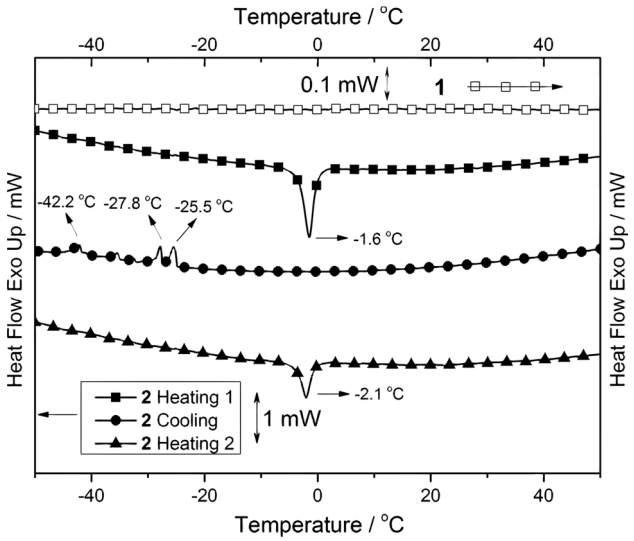

Fig. 12 Phase transitions of the ligand **1** and **2** by DSC

small exothermic peaks appear due to the time necessary for nucleation. On the second heating, the endothermic peak at −2.1 °C refers to a reversible phase transition. However, under dynamic conditions the transformation between phases is not entirely complete. In complexes **I** and **II**, no phase transition was detected.

Biological activity

Toxicity of I and II on Caco-2 cells

MTT viability and LDH cell toxicity tests were used to determine the non-toxic concentrations on Caco-2 human intestinal epithelial cells. From the hcmp ligand series for 3, no cell damaging effect was measured by MTT assay for 24-h treatment in the concentration ≤1000 μM. Complex formation notably enhanced the biological activity of the ligand, and the toxic concentration was more than 30 times higher on Caco-2 cells for both I and II (≥30 μM) measured by a metabolic assay. With LDH assay, a significant release of LDH was observed at 1 μM and higher concentrations of **II** in Caco-2 cells. On the contrary, despite the minor structural differences between **I** and **II**, the release of LDH in the solution of complex **I** started only by increasing its concentration to above 30 μM.

Conclusions

In aqueous solution, in the presence of sodium acetate, the monohydrate of *hcmp*·H_2O is obtained in the form of polymorph **1**, while in ethanolic solution the anhydrous *hcmp* (**3**) is crystallized. The reaction of the *hcmp* with $MgCO_3$ instead of coordination resulted in a formation a new polymorph of *hcmp*·H_2O (**2**). Depending on the reaction conditions, two stable polymorphs of zinc complex were isolated. The polymorphism in both cases depends on the reaction conditions, namely on the ions, which do not take part in complex formation.

Comparison of intramolecular energies of **1**–**3** shows that intramolecular energy decreases in the order **1** > **2** > **3**. Examination of the strength of pairwise molecule–molecule interactions indicates that in **1** and **2**, the aggregation of molecules into chains gives the main contribution to the stability of crystal lattice. Water molecules located between the chains interact with these chains with much lower energy. In **3**, molecules are packed in herringbone fashion with dominant contribution of electrostatic forces to the stabilization of crystal lattice. Main structural difference between **1** and **2** is the different mode of aggregation of the otherwise similar molecular chains. This is caused by different interchain nonbonding interactions and particularly by the presence of stacking interactions in **1**, between the two pyrazole rings supported by four nonbonding O–H···N H-bonds. In **2**, there are no stacking interactions and the link between the chains is achieved by the pair of O–H···N H-bonds. Interestingly, the presence of stacking interactions supported by hydrogen bonds did not lead to larger temperature of dehydration of the compound **1**, relative to **2**. It is significant to note the same mutual orientation of the pyrazole rings involved in stacking interactions in **1**, **I** and **II**. In all three cases, pyrazole rings are oriented in antiparallel fashion.

Analysis of intermolecular contacts in **I** and **II** and visual inspection of the resulting molecular aggregation suggest the key role of the coordinated water in the formation of two polymorphic forms, **I** and **II**. Enhanced hydrogen bonding capacity of coordinated water in **II** relative to **I** is associated with the formation of multistacked chain of molecules in **II**.

Despite the similar structures, the dehydration appears at somewhat higher temperatures in **2** than in **1**, while the stability of the dehydrated **1** is somewhat higher (252 and 248 °C onsets for **1** and **2**). The decomposition temperature of the anhydrate form **3** starts at 230 °C. This indicates that the stability of the compounds decreases in the order **3** > **2** > **1**. Both the monohydrate complexes **I** and **II** loose the crystal water at room temperature. The only significant difference in decomposition scheme is in the rate of the first decomposition step that is higher in **II**.

No significant biological activity was found in *hcmp* ligands. The toxicity of the zinc(II) complexes **I** and **II** is considerably higher. In spite of the high similarity in their structures, polymorph **II** shows a markedly higher release of LDH compared to that of **I**.

Acknowledgments This work was supported by the Ministry of Education and Science of the Republic of Serbia (continuation of the project No. 172014). The authors thank Dr Slađana B. Novaković for helpful discussions.

References

1. Keter FK, Darkwa J (2012) Biometals 25:9–21
2. Kulkarni NV, Revankar VK (2011) J Coord Chem 64:725–741
3. Manikannan R, Venkatesan R, Muthusubramanian R, Yogeeswari P, Sriram D (2010) Bioorg Med Chem Lett 20:6920–6924
4. Fonteh PN, Keter FK, Meyer D, Guzei IA, Darkwa J (2009) J Inorg Biochem 103:190–194
5. Sharma KV, Sharma V (2008) Asian J Chem 20:6213–6216
6. Eissa AAM, Farag NAH, Soliman GAH (2009) Bioorg Med Chem 17:5059–5070
7. Wang H, Luo X, Hou MYJ, Robinson H, Ke H (2010) J Med Chem 53:1726–1731
8. Tripathi UN, Venubabu G, Ahmad MS, Kolisetty SSR, Srivastava AK (2006) Appl Organomet Chem 20:669–676
9. Tripathi UN, Ahmadz MS, Venubabuz G, Ramakrishna P (2007) J Coord Chem 60:1777–1788
10. Yousef TA, Abu El-Reash GM, Al-Jahdali M, Bastawesy E, El-Rakhawy R (2014) Spectrochim Acta A 129:163–172
11. Holló B, Rodić MV, Bera O, Jovičić M, Leovac VM, Tomić ZD, Mészáros Szécsényi K (2013) Struct Chem 24:2193–2201
12. Mészáros Szécsényi K, Leovac VM, Češljević VI, Kovács A, Pokol G, Argay G, Kálmán A, Bogdanović GA, Jaćimović ŽK, Spasojević-de Biré A (2003) Inorg Chim Acta 353:253–262
13. Ristić IS, Barta Holló B, Budinski-Simendić J, Mészáros Szécsényi K, Cakić S, Szilágyi IM, Pokol G (2015) J Therm Anal Calorim 119:1011–1021
14. Steed JW (2013) Trends Pharmacol Sci 34:185–193
15. Polavarapu L, Mourdikoudis S, Pastoriza-Santos I, Pérez-Juste J (2015) CrystEngComm 17:3727–3762
16. Erkin AV, Krutikov VI (2009) Russ J Gen Chem 79:1204–1209
17. Oxford Diffraction (2008) CrysAlis CCD and CrysAlis RED Versions 1.171.32.24. Oxford Diffraction Ltd, Abington
18. Oxford Diffraction (2008) CrysAlisPro Version 1.171.32.24. Oxford Diffraction Ltd, Abington
19. Altomare A, Cascarano G, Giacovazzo C, Guagliardi A (1993) J Appl Crystallogr 26:343–350
20. Farrugia LJ (1999) J Appl Crystallogr 32:837–838
21. Sheldrick GM (2008) Acta Crystallogr A 64:112–122
22. Farrugia LJ (1997) J Appl Crystallogr 30:565–566
23. Watkin DJ, Prout CK, Pearce LJ (1996) CAMERON chemical crystallography laboratory. University of Oxford, Oxford
24. Bruno J, Cole JC, Edgington PR, Kessler MK, Macrae CF, McCabe P, Pearson J, Taylor R (2002) Acta Crystallogr B 58:389–397
25. Spek ALJ (2003) J Appl Crystallogr 36:7–13
26. Gavezzotti A (2003) J Phys Chem B107:2344–2353
27. Frisch MJ, Trucks GW, Schlegel HB, Scuseria GE, Robb MA, Cheeseman JR, Scalmani G, Barone V, Mennucci B, Petersson GA, Nakatsuji H, Caricato M, Li X, Hratchian HP, Izmaylov AF, Bloino J, Zheng G, Sonnenberg JL, Hada M, Ehara M, Toyota K, Fukuda R, Hasegawa J, Ishida M, Nakajima T, Honda Y, Kitao O, Nakai H, Vreven T, Montgomery JA, Peralta JE, Ogliaro F, Bearpark M, Heyd JJ, Brothers E, Kudin KN, Staroverov VN, Kobayashi R, Normand J, Raghavachari K, Rendell A, Burant JC, Iyengar SS, Tomasi J, Cossi M, Rega N, Millam JM, Klene M, Knox JE, Cross JB, Bakken V, Adamo C, Jaramillo J, Gomperts R, Stratmann RE, Yazyev O, Austin AJ, Cammi R, Pomelli C, Ochterski JW, Martin RL, Morokuma K, Zakrzewski VG, Voth GA, Salvador P, Dannenberg JJ, Dapprich S, Daniels AD, Farkas O, Foresman JB, Ortiz JV, Cioslowski J, Fox DJ (2009) Gaussian 09 Rev. A.1 Gaussian Inc. Wallingford CT
28. Gavezzotti A (2008) Mol Phys 106:1473–1485
29. C-Y Zheng, Wang DJ, Fan L, Zheng J (2013) Struct Chem 24:705–711
30. Geary WJ (1971) Coord Chem Rev 7:81–122
31. Allen FH, Motherwell WDS (2002) Acta Cryst B58:407–422
32. Gavezzotti A (2013) CrystEngComm 15:4027–4035
33. Kitaigorodskii AI (1973) Molecular crystals and molecules. Academic Press, New York
34. Gavezzotti A (2014) The Coulomb–London–Pauli (CLP) model of intermolecular interaction, description and user's manual. Dipartimento di Chimica Università di Milano
35. Addison AW, Rao TN, Reedijk J, Rijn JV, Verschoor CG (1984) J Chem Soc Dalton Trans 1349–1356. http://pubs.rsc.org/en/journals/journalissues/dt?issueid=dt1984_0_7&issnprint=0300-9246#!issueid=dt1984_0_7&type=archive&issnprint=0300-9246
36. Giron D, Monnier S, Mutz M, Piechon P, Buser T, Stowasser F, Schulze K, Bellus M (2007) J Therm Anal Calorim 89:729–743
37. Hino T, Ford JL, Powell MW (2001) Thermochim Acta 374:85–92